

# Supplementary Materials

## Interfacial electronic rearrangement and synergistic catalysis for alkaline water splitting in carbon encapsulated Ni (111)/Ni<sub>3</sub>C (113) heterostructure

Xiaoyu Li,<sup>a†</sup> Zhenbo Peng,<sup>b†</sup> Dongmei Jia,<sup>a†</sup> Yikang Wang,<sup>a</sup> Wenbo Wu,<sup>a</sup> Ping Deng,<sup>a</sup> Mengqiu Xu,<sup>a</sup> Xudong Xu,<sup>a</sup> Gan Jia,<sup>a</sup> Liang Chen,<sup>a</sup> Wei Ye<sup>a</sup> and Peng Gao<sup>\*a</sup>

<sup>a</sup> College of Material, Chemistry and Chemical Engineering, Hangzhou Normal University, Hangzhou 311121, Zhejiang, P. R. China.

<sup>b</sup> Zhejiang Collaborative Innovation Center for High Value Utilization of Byproducts from Ethylene Project, Ningbo Polytechnic, Ningbo 315800, Zhejiang, P. R. China

<sup>†</sup> These authors contributed equally to this work.

\* Corresponding author (E-mail: gaopeng@hznu.edu.cn)

## Experimental section

### Preparation of working electrode

For powders, they were coated on carbon paper using Nafion as binder: 5mg electrocatalyst and 50  $\mu\text{L}$  Nafion (5 wt.% in a mixture of lower aliphatic alcohol and water, Aldrich Chemical) were dispersed in 1 mL water/ethanol (volume ratio, 3:1) solution by sonication to form a dispersion. The mixed solution was sonicated for 5 min to obtain a homogeneous catalyst ink. The dispersion (105  $\mu\text{L}$ ) was pipetted onto a piece of clean carbon paper (1 cm  $\times$  1 cm), which was subject to overnight solvent evaporation in air. The mass of powders was controlled to obtain a loading amount of 0.50 mg  $\text{cm}^{-2}$ . The working electrode was dried at ambient temperature before electrochemical measurements. Linear sweep voltammetry was conducted in  $\text{N}_2$  saturated 1.0 M KOH with a scan rate of 5  $\text{mV s}^{-1}$ .

### Computational details

Spin-polarized density functional theory (DFT) method was employed by the Vienna Ab initio Simulation Package (VASP).[1, 2] The cut-off energy of 450 eV and k-points grids of  $3 \times 1 \times 1$  was used for the plane-wave expansion and Brillouin-zone, and the generalized gradient approximation (GGA) in the form of the Perdew-Burke-Ernzerh of (PBE) functional was set to describe the electron exchange-correlation energy.[3] During geometry optimization, the convergence criteria of energy and force were set to  $1 \times 10^{-4}$  eV and 0.02 eV/ $\text{\AA}$ , respectively. A vacuum region of 15  $\text{\AA}$  along the z direction was added to avoid the interaction in adjacent periodic images. The DFT-D3 method was applied to describe the correction of van der Waals interaction.[4, 5] Thermodynamic analysis of each reaction step was calculated by the change of Gibbs free energy ( $\Delta G$ ) by employing the computational hydrogen electrode model,[6, 7] where the chemical potential of the  $\text{H}^+/\text{e}^-$  pairs is equal to half of that of  $\text{H}_2$  molecule. The change of Gibbs free energy can be calculated as follows:

$$\Delta G = \Delta E + \Delta E_{\text{zpe}} - T\Delta S$$

where  $\Delta E$ ,  $\Delta E_{\text{zpe}}$  and  $\Delta S$  is the electronic energy difference, the correction of zero-point energy (ZPE) difference and the entropy change between the product and reactant species, and T is the temperature (298.15 K). The zero-point energy and entropy were determined by the vibrational frequency calculations.

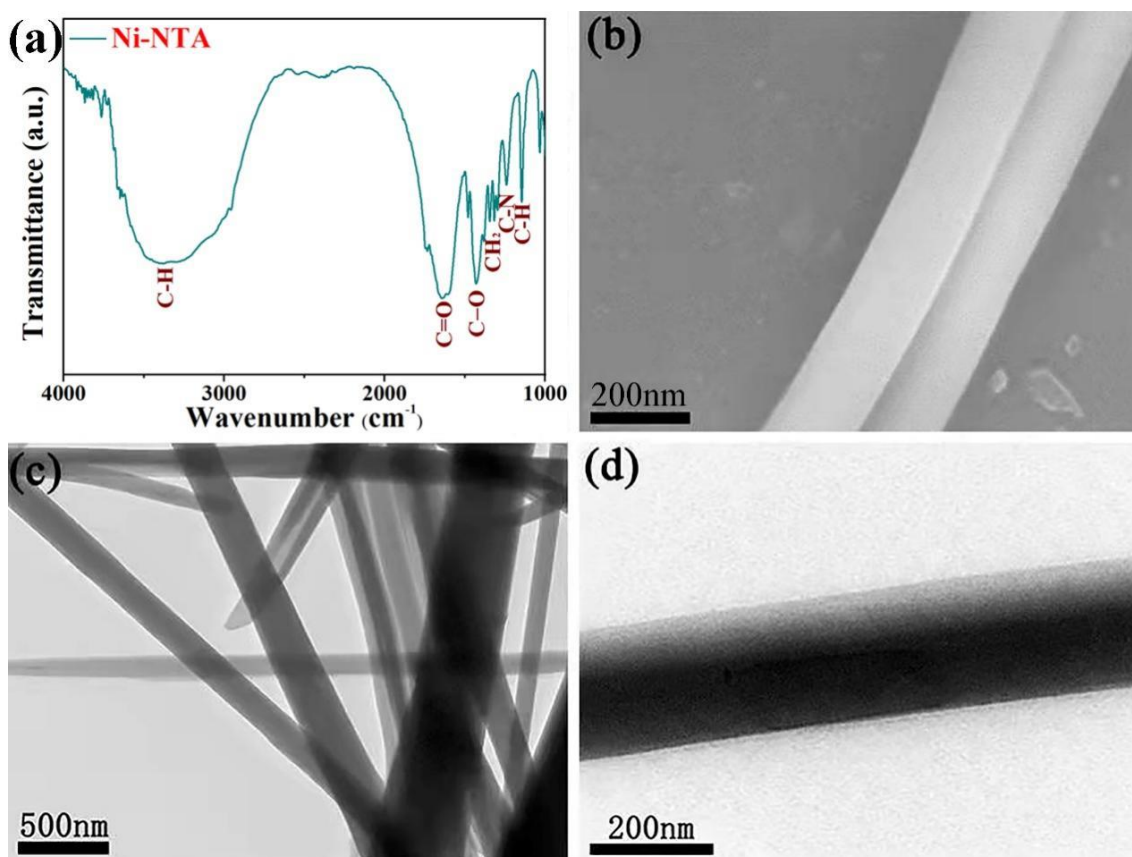


**Figure S1** Microstructure and composition characterizations of the as-obtained Ni-NTA precursor. (a) FT-IR spectrum; (b) SEM images; (c-d) TEM images.

FT-IR result exhibits a strong absorption peak at  $1644\text{ cm}^{-1}$ , which is attribute to the stretching vibration of C=O in linear polyamide. Furthermore, the peaks at  $3477$  and  $3270\text{ cm}^{-1}$  according to C-H also prove the formation of linear polyamide. In addition, the Ni-NTA precursor also shows obvious strong peaks for C-O, CH<sub>2</sub>, C-N and C-H groups at  $1425$ ,  $1348$ ,  $1291$  and  $1135\text{ cm}^{-1}$ , respectively.[8, 9] This FT-IR result proves the linear polymerization between NTA molecules, which leads to the one-dimensional structure of the Ni-NTA product.

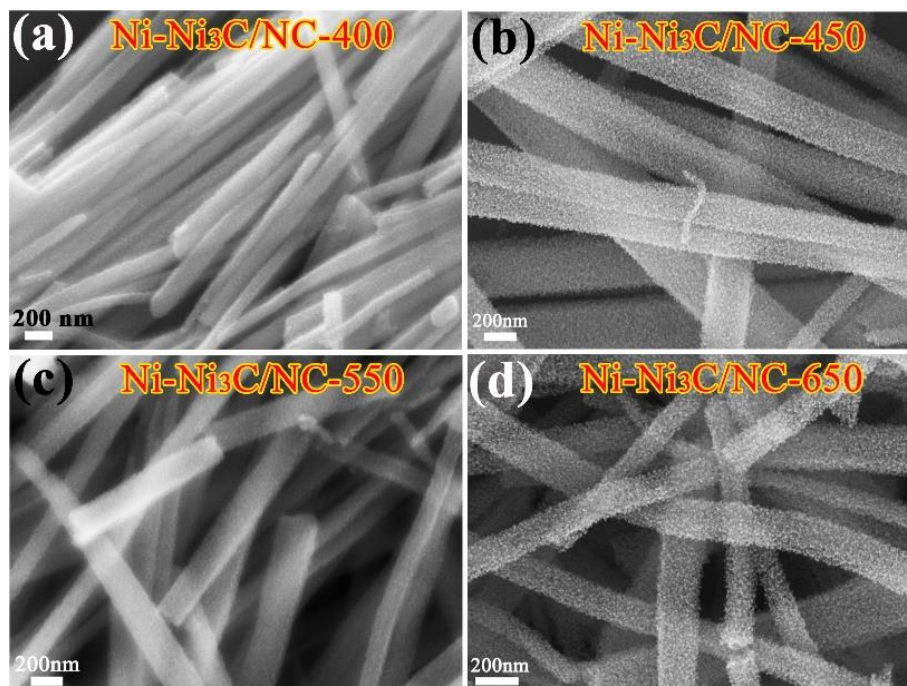


**Figure S2** SEM images of (a) Ni-Ni<sub>3</sub>C/NC-400, (b) Ni-Ni<sub>3</sub>C/NC-450, (c) Ni-Ni<sub>3</sub>C/NC-550, and (d) Ni-Ni<sub>3</sub>C/NC-650.

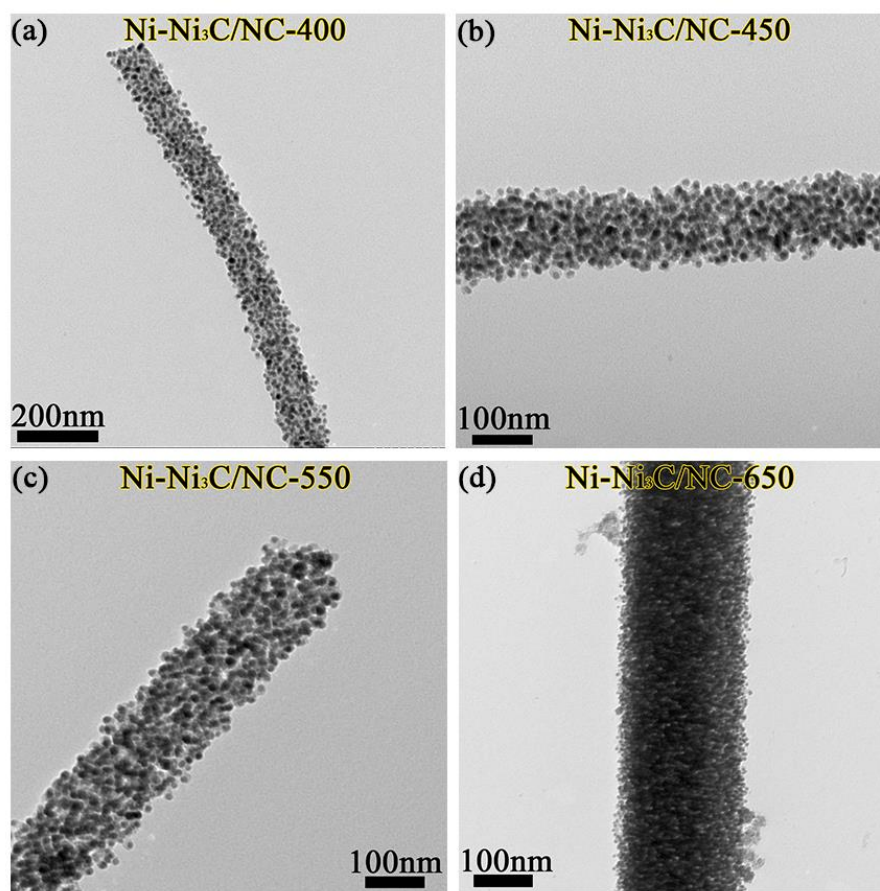


**Figure S3** TEM images of the (a) Ni-Ni<sub>3</sub>C/NC-400, (b) Ni-Ni<sub>3</sub>C/NC-450, (c) Ni-Ni<sub>3</sub>C/NC-550 and (d) Ni-Ni<sub>3</sub>C/NC-650.

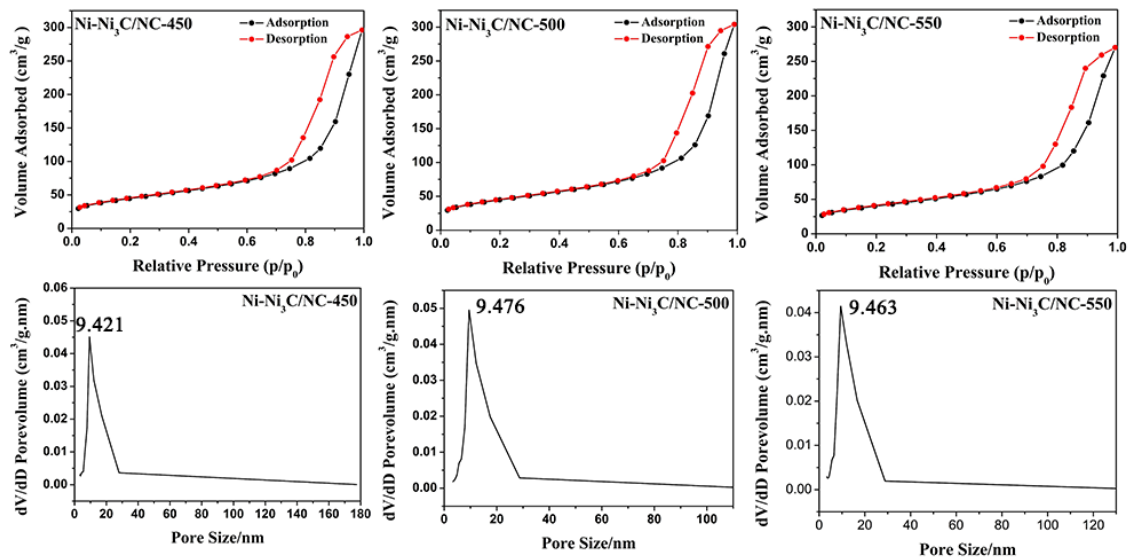


**Figure S4** (a-c)  $N_2$  adsorption-desorption isotherms and (d-f) pore-size distribution curves of the Ni-Ni<sub>3</sub>C/NC-450, Ni-Ni<sub>3</sub>C/NC-500 and Ni-Ni<sub>3</sub>C/NC-550.

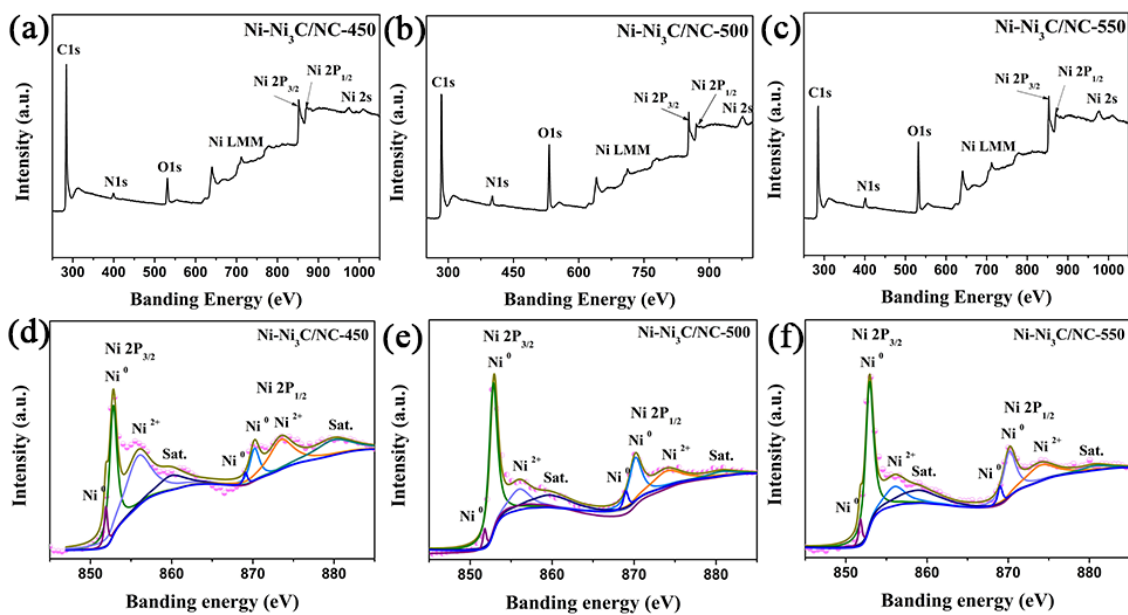


**Figure S5** XPS spectra of Ni-Ni<sub>3</sub>C/NC-450, Ni-Ni<sub>3</sub>C/NC-500 and Ni-Ni<sub>3</sub>C/NC-550: (a-c) Full XPS spectra; (d-f) Their entire Ni 2p spectra.

Note: the atomic ratios of C, N and Ni of Ni-Ni<sub>3</sub>C/NC-450 is 88.81%, 4.02% and 7.18%; the atomic ratios of C, N and Ni of Ni-Ni<sub>3</sub>C/NC-500 is 87.46%, 6.37% and 6.17%; the atomic ratios of C, N and Ni of Ni-Ni<sub>3</sub>C/NC-550 is 83.73%, 7.55% and 8.72%.



**Figure S6** The equipment picture of alkaline HER test in 1 M KOH solution.

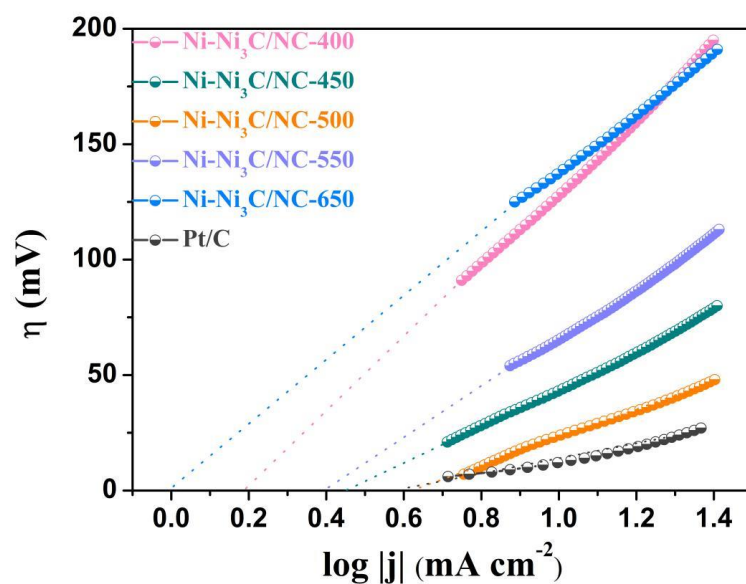


**Figure S7** Exchange current densities ( $j_0$ ) of Ni-Ni<sub>3</sub>C/NC-400, Ni-Ni<sub>3</sub>C/NC-450, Ni-Ni<sub>3</sub>C/NC-500, Ni-Ni<sub>3</sub>C/NC-550, Ni-Ni<sub>3</sub>C/NC-650 and Pt/C, are determined by using extrapolation method.

Note: In this way,  $j_0$  values of Ni-Ni<sub>3</sub>C/NC-400, Ni-Ni<sub>3</sub>C/NC-450, Ni-Ni<sub>3</sub>C/NC-500, Ni-Ni<sub>3</sub>C/NC-550, Ni-Ni<sub>3</sub>C/NC-650 and Pt/C were determined to be 1.2, 1.56, 2.54, 2.94, 4.13 and 3.97 mA cm<sup>-2</sup>, respectively.

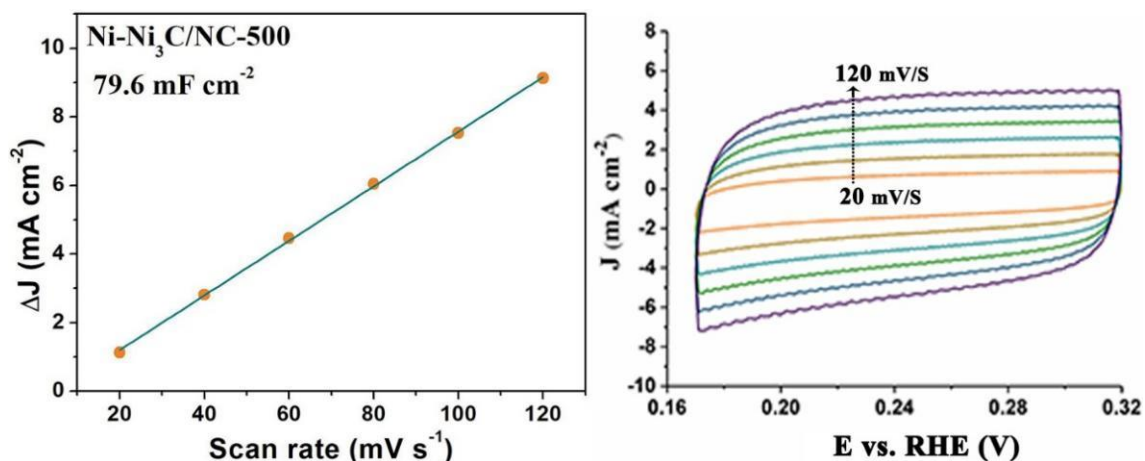


Figure S8 The extraction of the  $C_{dl}$  and CV with different rates (20~120 mV/S) for Ni-Ni<sub>3</sub>C/NC-500.

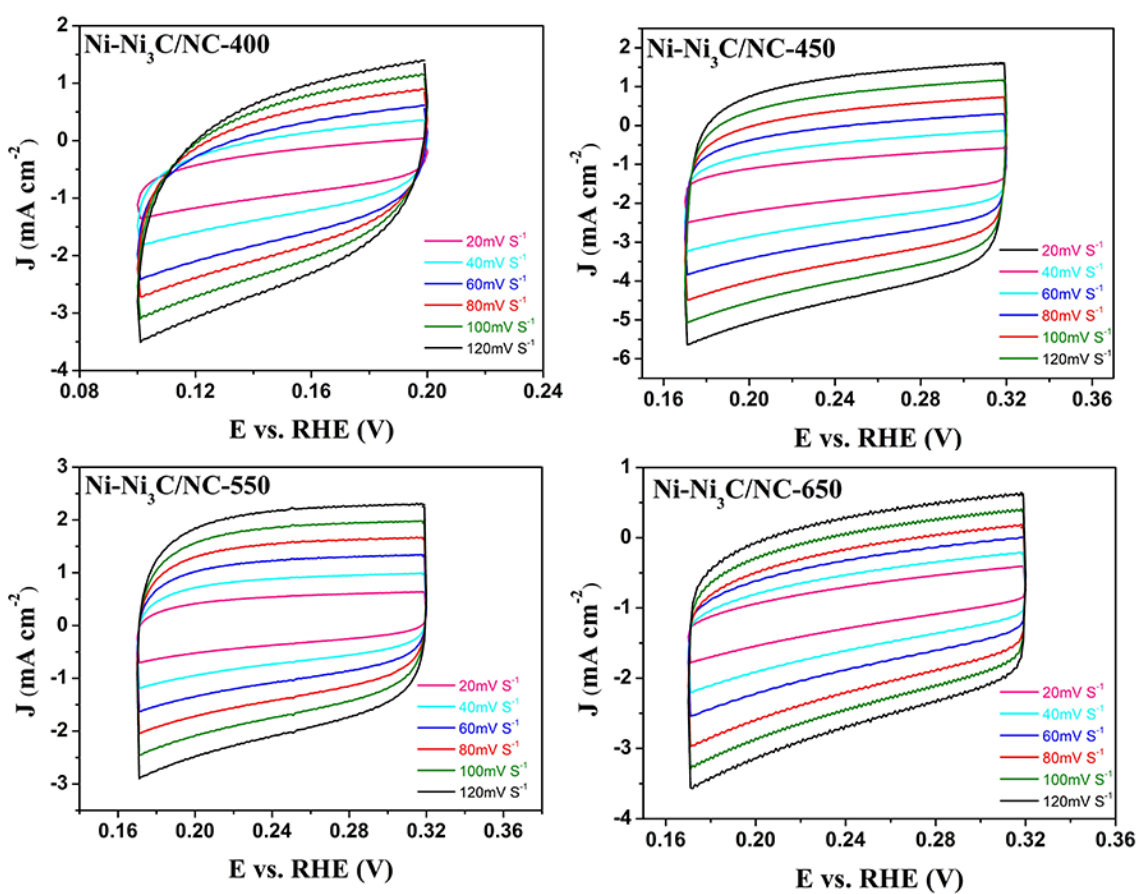
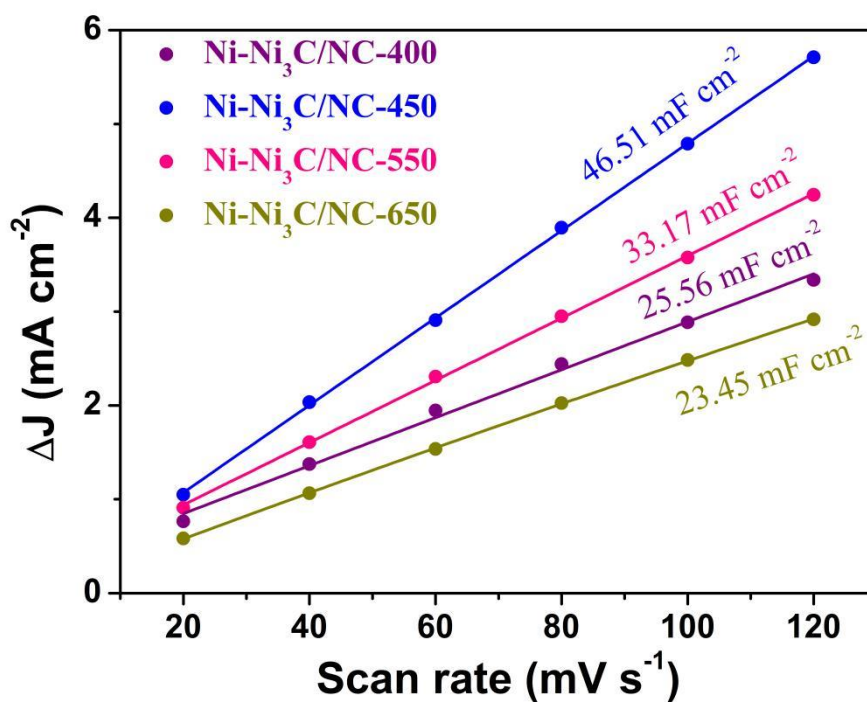
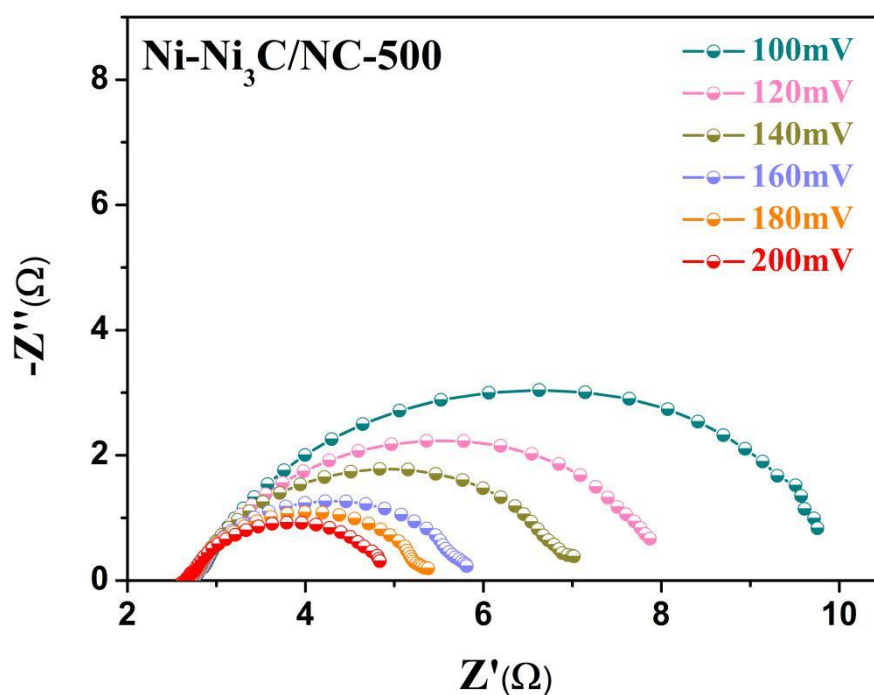


Figure S9 CV curves for calculation of double-layer capacitance. CV curves of Ni-Ni<sub>3</sub>C/NC-400, Ni-Ni<sub>3</sub>C/NC-450, Ni-Ni<sub>3</sub>C/NC-550, Ni-Ni<sub>3</sub>C/NC-650 at scan rates ranging from 20 mV S<sup>-1</sup>.



**Figure S10** The capacitive current densities measured at 0.25 V vs RHE with different scan rates.

**Note:** The specific capacitance obtained in Figure 4f can be converted into an electrochemical active surface area (ECSA) using the specific capacitance value for a flat standard with 1 cm<sup>2</sup> of real surface area. The specific capacitance for a flat surface is generally found to be in the range of 20-60 μF cm<sup>-2</sup>. Here we assume 40 μF cm<sup>-2</sup>. The ECSA of Ni-Ni<sub>3</sub>C/NC-400, Ni-Ni<sub>3</sub>C/NC-450, Ni-Ni<sub>3</sub>C/NC-550, and Ni-Ni<sub>3</sub>C/NC-650 are 1162 cm<sup>2</sup>, 829 cm<sup>2</sup>, 639 cm<sup>2</sup> and 586 cm<sup>2</sup>, respectively.



**Figure S11** The corresponding Nyquist plots of Ni-Ni<sub>3</sub>C/NC-500 at various voltages in 1M KOH.

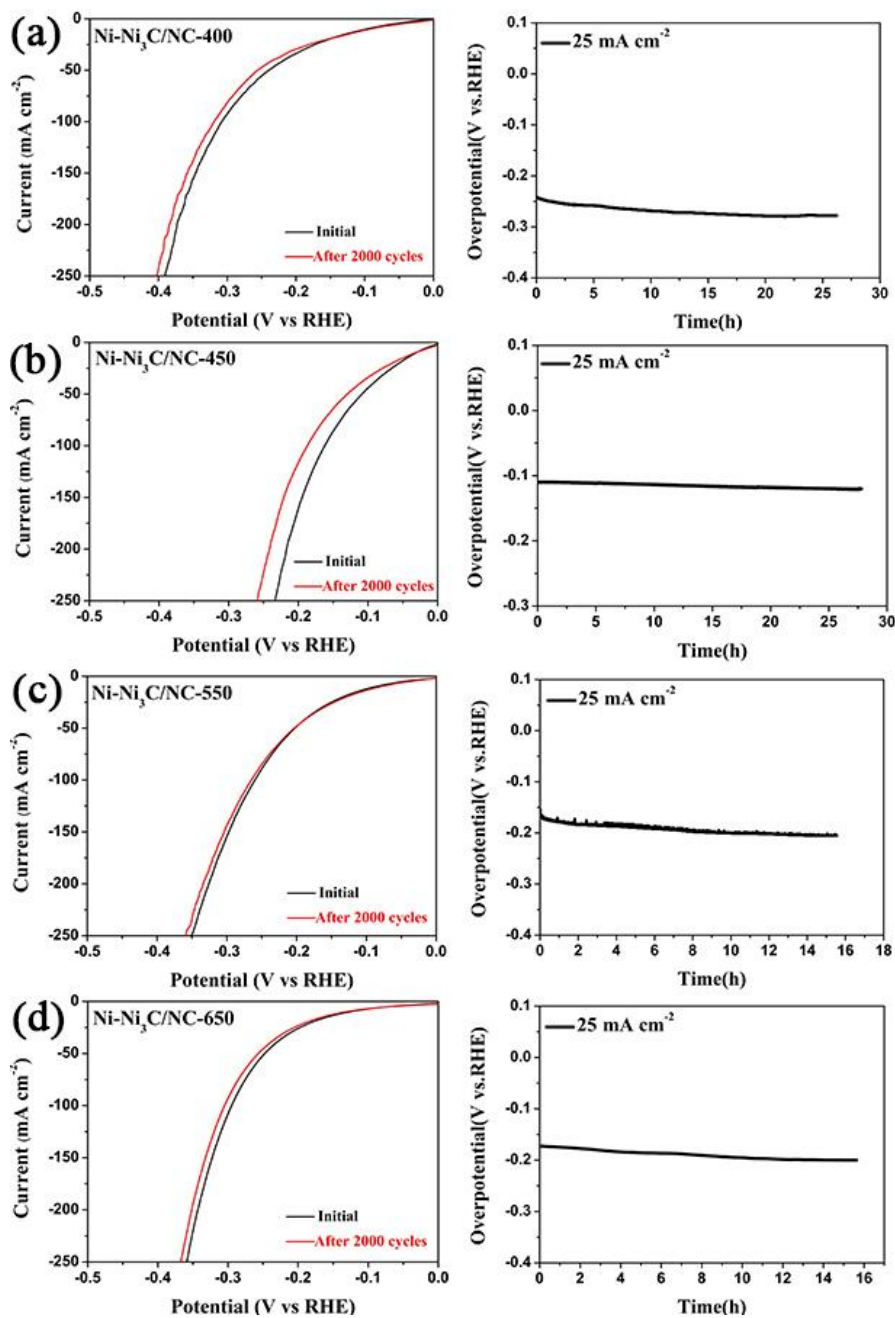


**Figure S12** Polarization curves before and after 2000 CV cycles and the long-term stability measurements of Ni-Ni<sub>3</sub>C/NC-400, Ni-Ni<sub>3</sub>C/NC-450, Ni-Ni<sub>3</sub>C/NC-550 and Ni-Ni<sub>3</sub>C/NC-650 at 25 mA cm<sup>-1</sup> constant current density.

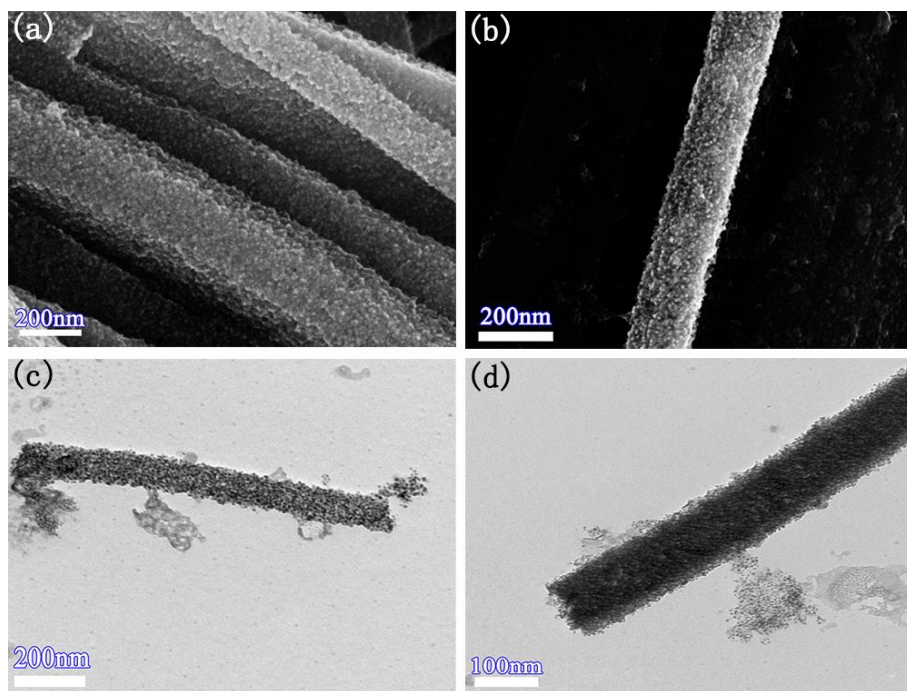


**Figure S13** (a, b) SEM micrograph, (c, d) TEM micrograph of Ni-Ni<sub>3</sub>C/NC-500 after a 100 h HER measurement.

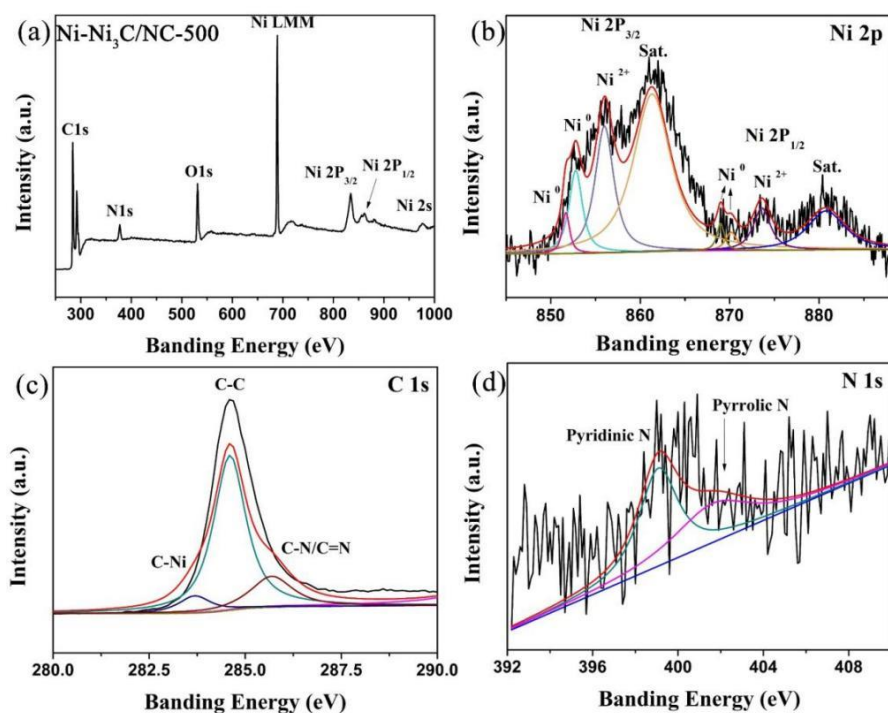


**Figure S14** XPS spectra of Ni-Ni<sub>3</sub>C/NC-500 after a 10 h long-term HER test.

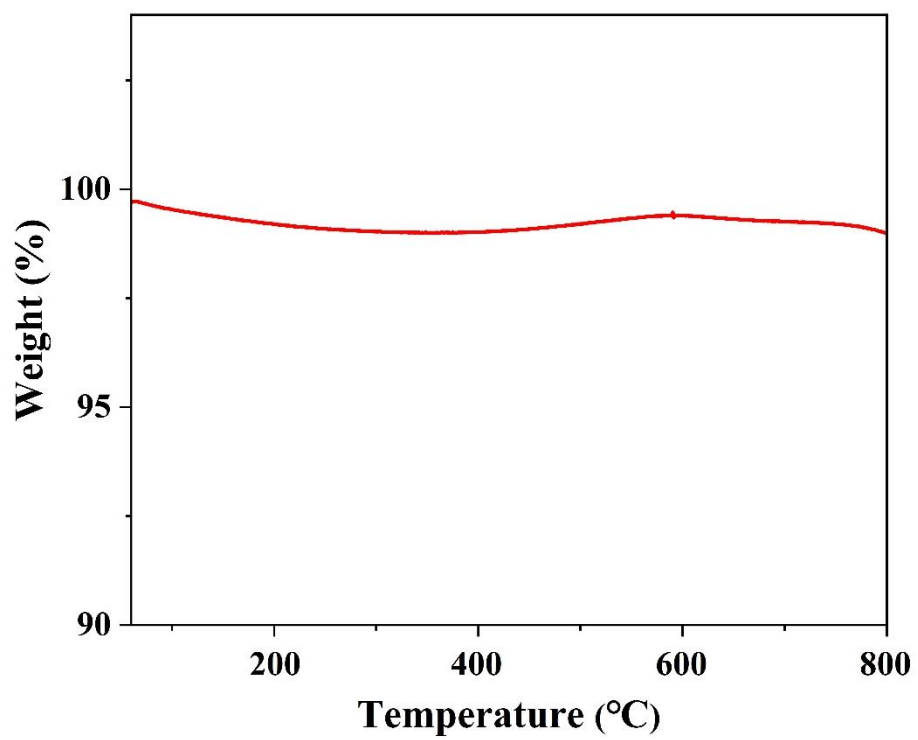


**Figure S15** Thermogravimetric analysis (TGA) curve of Ni - Ni<sub>3</sub>C/NC-500.

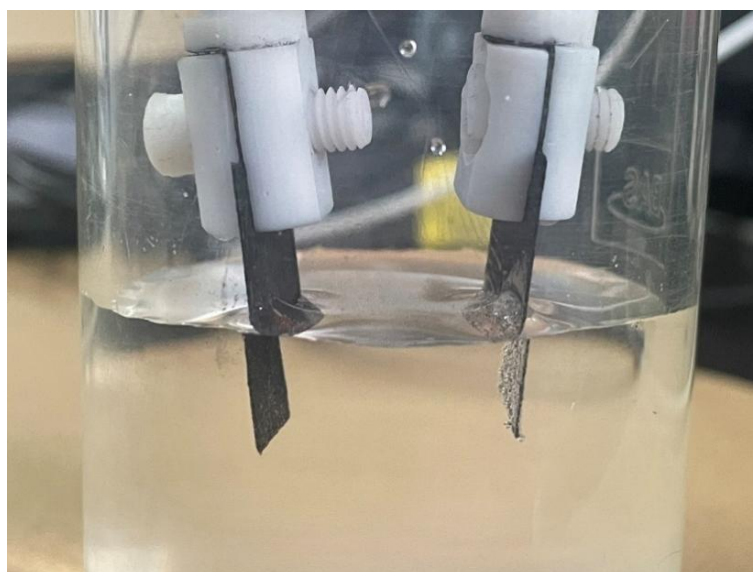


**Figure S16** The equipment picture of alkaline OWS test in 1 M KOH solution.

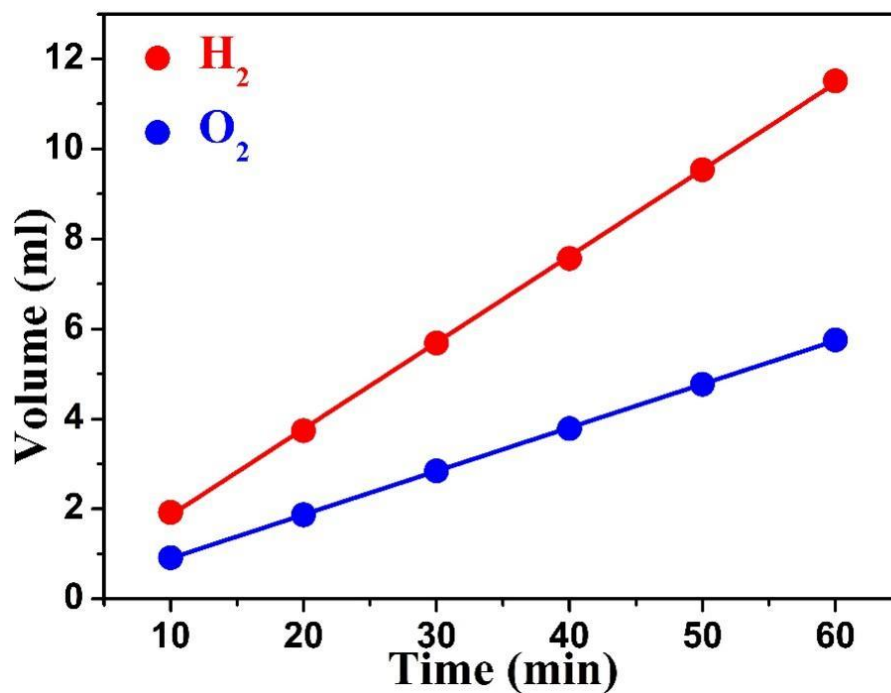


**Figure S17** The volumes of H<sub>2</sub> and O<sub>2</sub> as a function of time in the electrocatalytic overall water splitting.

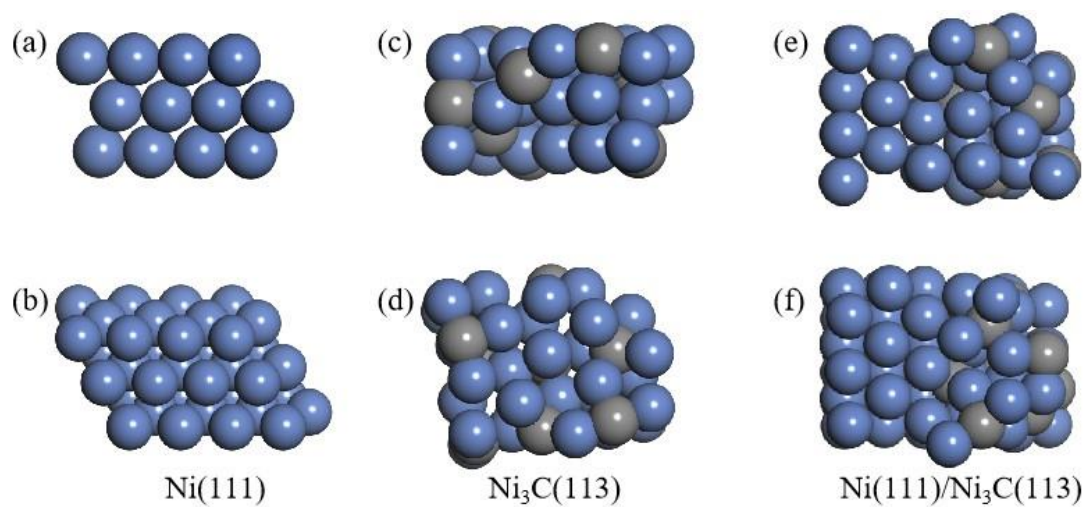


**Figure S18** Side (top) and top (bottom) view of three surfaces, including Ni (111), Ni<sub>3</sub>C (113) and Ni (111)/Ni<sub>3</sub>C (113).

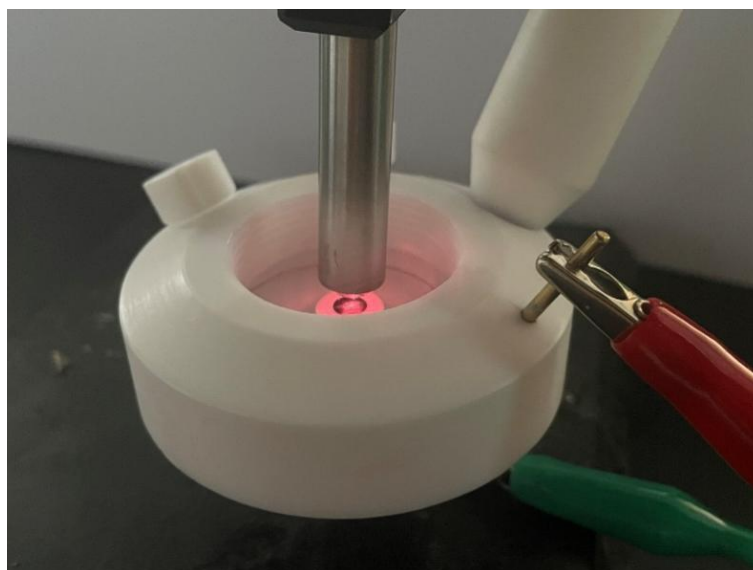


**Figure S19** The equipment picture of in-situ electrochemical Raman spectrum.

**Table S1** N<sub>2</sub> adsorption-desorption isotherms and pore-size distribution curves of the Ni-Ni<sub>3</sub>C/NC-450, Ni-Ni<sub>3</sub>C/NC-500 and Ni-Ni<sub>3</sub>C/NC-550.

<b>Sample</b>	<b>Ni-Ni<sub>3</sub>C/NC-450</b>	<b>Ni-Ni<sub>3</sub>C/NC-500</b>	<b>Ni-Ni<sub>3</sub>C/NC-550</b>
Adsorption-desorption isotherms (m <sup>2</sup> /g)	156.925	160.478	143.113
Pore-size (nm)	9.421	9.476	9.463

**Table S2** Comparison of catalytic parameters of Ni–Ni<sub>3</sub>C/NC-500 and other Ni-based HER composite-catalysts in alkaline media.

Catalyst	Loading density (mg cm <sup>-2</sup> )	Electrolyte	Overpotential at 10 mA cm <sup>-2</sup> (mV)	Tafel slope (mV dec <sup>-1</sup> )	Reference
NiP <sub>2</sub> /NiO NRs	0.24	1M KOH	131	94	<i>ACS Appl. Mater. Interfaces</i> , <b>2018</b> , 10,17896.
Ni <sub>3</sub> C/CNT	3.0	1M KOH	132	49	<i>J. Mater. Chem. A</i> , <b>2018</b> , 6, 4297.
Ni <sub>3</sub> N@CQDS	0.18	1M KOH	77	91	<i>ACS nano</i> , <b>2018</b> , 12, 4148.
Ni/Ni <sub>3</sub> C–NCNT	0.5	1M KOH	184	98.7	<i>Chem. Front.</i> , <b>2019</b> , 6, 1073.
Ni–Ni <sub>3</sub> C/CC	3.0	1M KOH	98	88.50	<i>Small</i> , <b>2020</b> , 16, 41.
NiO <sub>x</sub> –AC–500	2.0	0.1M KOH	180	121	<i>Carbon</i> , <b>2020</b> , 157, 515–524.
SGNCs–900	0.6	1M KOH	27	38	<i>Nano Lett.</i> , <b>2020</b> , 20, 8375.
D–Ni–MOF	0.15	1M KOH	101	50.9	<i>Small</i> , <b>2020</b> , 16, 41.
N–NiCo–LDH–6	/	1M KOH	35	34	<i>J. Mater. Chem. A</i> , <b>2021</b> , 9, 10260–10269.
Ni–M@C–130	0.28	1M KOH	123	50.8	<i>ACS Sustainable Chem. Eng.</i> <b>2021</b> , 9, 4, 1920–1931.
WN–Ni@N, P–CNT–800	1.0	1M KOH	73	151.7	<i>Appl. Catal. B: Environ.</i> , <b>2021</b> , 298, 120511.
Ni@NCNTs/NF–L	/	1M KOH	81	64.2	<i>Appl. Catal. B: Environ.</i> , <b>2021</b> , 283, 119674.
<b>Ni–Ni<sub>3</sub>C/NC</b>	<b>0.5</b>	<b>1M KOH</b>	<b>29</b>	<b>59.36</b>	<b>This work.</b>

**Table S3** Comparison of catalytic parameters of Ni–Ni<sub>3</sub>C/NC-500 and other Ni-based OER composite-catalysts in alkaline media.

Catalyst	Loading density (mg cm <sup>-2</sup> )	Electrolyte	Overpotential at 10 mA cm <sup>-2</sup> (mV)	Tafel slope (mV dec <sup>-1</sup> )	Reference
Ni–Co–P HNBs	2.0	1M KOH	270	76	<i>Energy Environ. Sci.</i> , <b>2018</b> , 11, 872.
Ni/Ni <sub>3</sub> C nanospheres	0.197	1M KOH	350	57.6	<i>Chem. Front.</i> , <b>2019</b> , 6, 1073.
Ni/Ni <sub>3</sub> C–NCNT	0.5	1M KOH	277	109.3	<i>Inorg. Chem. Front.</i> , <b>2019</b> , 6, 1073.
Ni <sub>3</sub> C/NC	0.297	1M KOH	309	72	<i>Electrochim. Acta</i> , <b>2019</b> , 320, 134631.
Ru/Ni <sub>3</sub> N–Ni	/	1M KOH	200	56.4	<i>Chem. Commun.</i> , <b>2020</b> , 56, 2352.
Ni–Ni <sub>3</sub> C/CC	3.0	1M KOH	268	43.8	<i>Small</i> , <b>2020</b> , 16, 2001642.
NiS/NF	/	1M KOH	173	80.15	<i>New J. Chem.</i> , <b>2020</b> , 45(4).
NaBH <sub>4</sub> –NiFe LDH	/	1M KOH	280	56	<i>RSC Adv.</i> , <b>2020</b> , 10, 33475–33482.
NiO <sub>x</sub>	/	1M KOH	358	73	<i>ACS Appl. Energy Mater.</i> <b>2021</b> , 4, 5255–5264.
Ni–M@C–130	0.28	1M KOH	244	47.2	<i>ACS Sustainable Chem. Eng.</i> , <b>2021</b> , 9, 4, 1920–1931.
NiFe–L	/	1M KOH	370	65.7	<i>Appl. Catal. B: Environ.</i> , <b>2021</b> , 283, 119674.
WN–Ni@N, P–CNT–800	1.0	1M KOH	268	59.8	<i>Appl. Catal. B: Environ.</i> , <b>2021</b> , 298, 120511.
<b>Ni–Ni<sub>3</sub>C/NC</b>	<b>0.5</b>	<b>1M KOH</b>	<b>267</b>	<b>81.99</b>	<b>This work.</b>

## References

1. Kresse, G.; Furthmüller, J., Efficient iterative schemes for ab initio total-energy calculations using a plane-wave basis set, *Physical Review B*, **1996**, 54, 11169-11186.
2. Kresse, G.; Joubert, D., From ultrasoft pseudopotentials to the projector augmented-wave method, *Physical Review B*, **1999**, 59, 1758-1775.
3. Perdew, J.P.; Burke, K.; Ernzerhof, M., Generalized Gradient Approximation Made Simple, *Physical Review Letters*, **1996**, 77, 3865-3868.
4. Grimme, S., Density functional theory with London dispersion corrections, *WIREs Computational Molecular Science*, **2011**, 1, 211-228.
5. Steinmann, S.N.; Corminboeuf, C., A System-Dependent Density-Based Dispersion Correction, *Journal of Chemical Theory and Computation*, **2010**, 6, 1990-2001.
6. Nørskov, J.K.; Bligaard, T.; Logadottir, A.; Kitchin, J.R.; Chen, J.G.; Pandelov, S.; Stimming, U., Trends in the Exchange Current for Hydrogen Evolution, *Journal of The Electrochemical Society*, **2005**, 152, J23.
7. Peterson, A.A.; Abild-Pedersen, F.; Studt, F.; Rossmeisl, J.; Nørskov, J.K., How copper catalyzes the electroreduction of carbon dioxide into hydrocarbon fuels, *Energy & Environmental Science*, **2010**, 3.
8. Tsuboi, M.; Onishi, T.; Nakagawa, I.; Shimanouchi, T.; Mizushima, S.-I., Assignments of the vibrational frequencies of glycine, *Spectrochimica Acta*, **1958**, 12, 253-261.
9. Reddy, A.L.M.; Shaijumon, M.M.; Gowda, S.R.; Ajayan, P.M., Coaxial MnO<sub>2</sub>/carbon nanotube array electrodes for high-performance lithium batteries, *Nano letters*, **2009**, 9, 1002-1006.